



Geophysical Research Letters

RESEARCH LETTER

10.1029/2019GL083881

Key Points:

- Variation in ice shelf basal melt rates is observed over a broad range of time scales, from tidal to seasonal
- Topographic shelf waves dominate the observed temporal melt rate variability in the study region
- Sea ice concentration and tidal currents modulate the magnitude and temporal variation of melt rates

Supporting Information:

- Supporting Information S1

Correspondence to:

S. Sun,
sainsun@ulb.ac.be

Citation:

Sun S., Hattermann, T., Pattyn, F., Nicholls, K. W., Drews, R., & Berger, S. (2019). Topographic shelf waves control seasonal melting near Antarctic ice shelf grounding lines. *Geophysical Research Letters*, 46, 9824–9832. <https://doi.org/10.1029/2019GL083881>

Received 27 MAY 2019

Accepted 13 AUG 2019

Accepted article online 19 AUG 2019

Published online 29 AUG 2019

Topographic Shelf Waves Control Seasonal Melting Near Antarctic Ice Shelf Grounding Lines

Sainan Sun¹ , Tore Hattermann² , Frank Pattyn¹ , Keith W. Nicholls³ , Reinhard Drews⁴ , and Sophie Berger⁵

¹Université libre de Bruxelles, Brussels, Belgium, ²Norwegian Polar Institute, Tromsø, Norway, ³British Antarctic Survey, Cambridge, UK, ⁴Department of Geosciences, University of Tübingen, Tübingen, Germany, ⁵Alfred Wegener Institute, Helmholtz-Centre for Polar and Marine Research, Bremerhaven, Germany

Abstract The buttressing potential of ice shelves is modulated by changes in subshef melting, in response to changing ocean conditions. We analyze the temporal variability in subshef melting using an autonomous phase-sensitive radio-echo sounder near the grounding line of the Roi Baudouin Ice Shelf in East Antarctica. When combined with additional oceanographic evidence of seasonal variations in the stratification and the amplification of diurnal tides around the shelf break topography (Gunnerus Bank), the results suggest an intricate mechanism in which topographic waves control the seasonal melt rate variability near the grounding line. This mechanism has not been considered before and has the potential to enhance local melt rates without advecting different water masses. As topographic waves seem to strengthen in a stratified ocean, the freshening of Antarctic surface water, predicted by observations and models, is likely to increase future basal melting in this area.

Plain Language Summary Ice shelves (or the floating parts of the Antarctic ice sheet) lose primarily mass through melting at their bottom in contact with the ocean. This thins them and makes them more vulnerable to potential collapse. To understand the processes governing such thinning, direct and long-time measurements are essential. Here we report on the first high-resolution time series of direct melt measurements on the Roi Baudouin Ice Shelf in Dronning Maud Land during 2016. We find that subshef melt varies on both seasonal and daily time scales. Temporal variations stem from topographical ocean waves that originate on the continental shelf and transfer ocean properties without time delay within the ice shelf cavity. Therefore, seasonal variations highly depend on the presence/absence of sea ice in front of the ice shelf, which impact the strength of topographical waves. This mechanism is highly efficient at increasing the ice-ocean exchanges and may explain regional differences in ice shelf melt.

1. Introduction

More than 75% of Antarctic continental ice discharges through ice shelves (Bindschadler et al., 2011) that buttress the grounded ice (Dupont & Alley, 2005). A reduction in ice shelf buttressing may lead to grounded ice flow acceleration (Rack & Rott, 2004; Reese et al., 2018; Schannwell et al., 2018). Numerical ice sheet models suggest that ice shelf thinning due to melting from their contact with warmer ocean waters could destabilize the ice sheet (Favier et al., 2014; Schannwell et al., 2018), indicating a crucial dependence of the ice sheet on processes at the ice-ocean interface. Here, we present new and highly resolving time series of melt rates observed on the Roi Baudouin Ice Shelf (RBIS), which is part of the belt of slowly melting (Rignot et al., 2013) smaller ice shelves situated over the narrow continental shelf along the coast of Dronning Maud Land, East Antarctica (Figure 1). The observations are taken near the grounding line where the bed lowers toward the interior of the ice sheet (Callens et al., 2014; Fretwell et al., 2013) and our analysis explores the oceanographic mechanisms that control basal melting in this region that is potentially susceptible to marine ice sheet instability (Favier et al., 2016).

Subshef melting depends on how fast energy can be transported across the boundary layer to the ice-ocean interface. Jacobs et al. (1992) present three possible sources that cause melting below Antarctic ice shelves. The first depends on the depression of the local freezing point with increasing pressure and depth: Even water that has been cooled to the surface freezing temperature may supply heat to melt the base of an ice shelf several hundred meters below sea level, driving the so-called ice pump circulation (Lewis & Perkin, 1986).

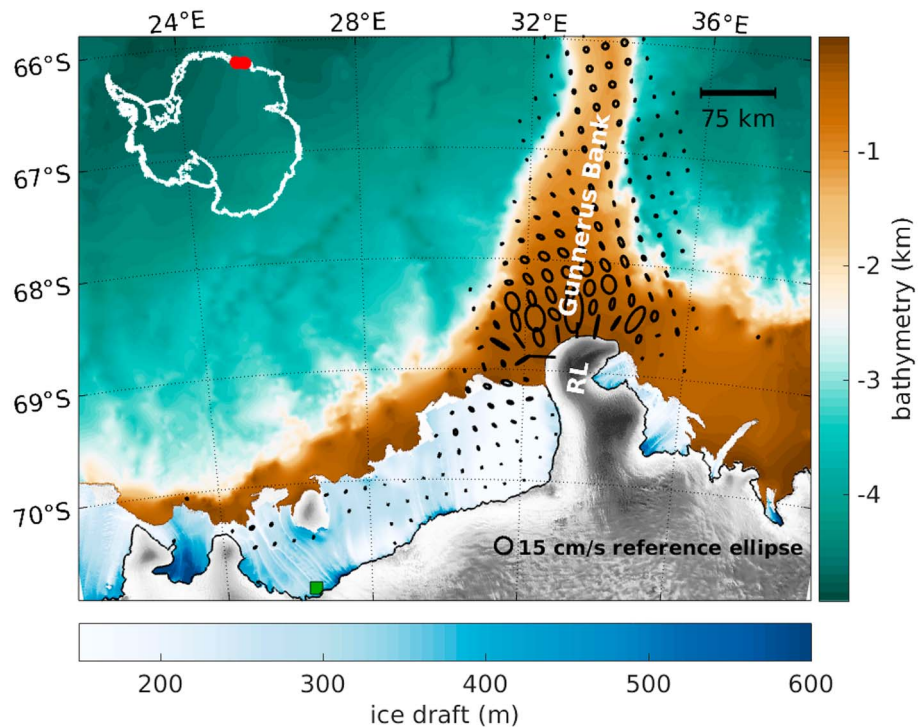


Figure 1. Overview of the study region. The background image is from a Radarsat mosaic (Jezek & RAMP-Product-Team, 2002), overlaid with the ice draft (Howat et al., 2019). The location of the ApRES on the Roi Baudouin Ice Shelf is indicated by the green square. The grounding line is plotted in black (Depoorter et al., 2013). Ocean bathymetry is from GEBCO_2014 (Weatherall et al., 2015), superimposed with tidal ellipses for the K1 constituent from the tide model CATS2008_opt where the amplitude of the semimajor axes is larger than 1.5 cm/s. RL denotes the Riiser-Larsen Peninsula. ApRES = autonomous phase-sensitive radio-echo sounder.

The second source is warm deep water from the Southern Ocean, which circulates along the continental shelf break. The third is the seasonally warmed Antarctic Surface Water (ASW), which could access the parts of the ice base close to the calving front.

The delivery of energy for each of the three sources is modulated by processes in the open ocean, as well as water circulation and transport in the ice shelf cavity (Dinniman et al., 2016; Stewart et al., 2018). The intrusion of warmer water into the ice shelf cavities along the Dronning Maud Land coast is strongly controlled by the depth of the Antarctic Slope Front thermocline (Hattermann, 2018) that is depressed below the shelf break by wind forcing (Heywood et al., 1998). The on-shore heat transport across the front is influenced by eddy overturning, freezing, and melting of sea ice (Hattermann et al., 2014; Nøst et al., 2011), and interactions with local topography (Dong et al., 2016). Persistent easterly winds along the entire coast of Dronning Maud Land (roughly between 30°E and 20°W) may push ASW into the ice shelf cavities (Zhou et al., 2014), affecting the coastal dynamics (Hattermann et al., 2012), and potentially increasing subshelf melting (Hattermann et al., 2014). Mixing of Warm Deep Water and ASW produces modified warm deep water (MWDW). Both ASW and MWDW are observed below the Fimbul Ice Shelf (Hattermann et al., 2012; Nøst et al., 2011) as well as below the RBIS (Callens, 2014).

Ambient ocean waters inside the ice shelf cavity mix with melt water at the ice/ocean boundary to form a buoyant plume that ascends in a boundary layer along the sloping ice base (Jenkins & Doake, 1991). Tidal currents contribute to the mixing of the water column and modify the hydrographic characteristics of the water masses at this boundary (Padman et al., 2018). They also strongly strengthen the turbulence at the ice-ocean interface, thereby increasing melting (or refreezing; Jourdain et al., 2019). For the Filchner-Ronne Ice Shelf, Makinson et al. (2011) show that including tidal forcing in a numerical ocean model leads to a threefold increase in the modeled melt rate. Furthermore, tides could trigger topographic waves over strong topographic slopes. They can be trapped (e.g., if the generation site is poleward of the critical latitude, which is the case for diurnal tidal constituents in Antarctica) or resonate with the natural modes of basins or bays

depending on ocean and topography characteristics and excite vigorous internal waves (Jensen et al., 2013; Semper & Darelius, 2017).

The purpose of this study is to investigate the ice-ocean interaction mechanisms driving subshelf melting for the RBIS, using an autonomous phase-sensitive radio-echo sounder (ApRES). The main advantage of this technique is the high vertical and temporal resolution of vertical strain variations that can be obtained (Nicholls et al., 2015), which enables melt rates at a high temporal resolution. An additional advantage is that the technique does not assume that the ice shelf is in steady state (Corr et al., 2002). Oceanographic data from the ambient environment is collected to aid in interpreting the temporal variability in melt rates. The observations give an insight into ice-ocean interaction mechanisms that mediate subshelf melting along the Dronning Maud Land coast. ApRES has been implemented in the other regions to derive time series of subshelf melt rates (Davis et al., 2018). This is the first occasion that time series of subshelf melt rates with such high temporal resolution have been obtained for this ice shelf. We explain the observed variability in basal melt rates using directly measurements of temporal variability in the ocean.

2. Data Collection and Processing

2.1. Subshelf Melt Rates Time Series From Radar Measurements

The ApRES (Brennan et al., 2014; Nicholls et al., 2015) was deployed from January to December in 2016 on the RBIS (Figure 1) about 90 km from the ice shelf front and 5 km seaward from the grounded ice on the fast-flowing portion of the West Ragnhild glacier, which is the third largest outlet glacier along the Dronning Maud Land Coast (Callens et al., 2014). The ice thickness at the site was ~ 300 m in the trough of a channel (Drews, 2015) but increases up to 600 m in the grounding zone upstream, and ice flow velocities in this region range between 250 and 300 m/a (Rignot et al., 2013). By transmitting an electromagnetic signal and receiving the echo, the radar system can detect the ice base (ice-ocean interface) as well as relatively weak internal reflecting layers that are due to changes in ice permittivity (Figure 2). Between two consecutive measurements, the relative vertical motion of internal layers and the base can therefore be tracked. The displacements of the internal layers determine how the thickness of the column evolves due to vertical strain and bottom melting (see below).

The equipment is described by Nicholls et al. (2015) and uses a Frequency Modulated Continuous Wave technique. It retains the phase of the echo, ensuring a high precision of the measurement, that is, a signal-to-noise ratio of 17 dB allows a 1° change in phase to be detectable, corresponding to a 1-mm change in range in the case of a system centered on 300 MHz (Nicholls et al., 2015). The generated chirp frequency ranges from 200 to 400 MHz. The bandwidth of 200 MHz gives a coarse range resolution of 43 cm in the vertical, and millimeter range precision can be achieved with relative phase measurements. A typical measurement lasts for 1–2 min. The instrument takes 20 measurements per hour to be averaged together and sleeps between measurements. The strength of the signal decreases with depth, leading to a larger error in the phase tracking for the deeper reflectors. Therefore, reflectors deeper than 250 m are not used because of the noise. The result is a clean linear fit, which is the expected behavior for a freely floating ice shelf. The gradient of the fitted line (Figure 2) gives the average vertical strain rate from the noncompacting ice, which is nearly the whole column due to the lack of firn cover in this area (Lenaerts et al., 2016). With both spatial and temporal fluctuations in the vertical strain rate accurately quantified, it is possible to estimate the vertical displacement of the ice shelf base in response to ice flow divergence. Differences between the predicted and observed motion of the basal reflector arise because of subshelf melting or accretion (Figure 2). All reflector displacements were processed using the method described by Brennan et al. (2014). Details of the assumptions and derivations are given by Jenkins et al. (2006).

2.2. Sea Ice and Ocean Properties

Time series of sea ice and ocean properties in this region are combined to determine the mechanisms controlling the subshelf melting. Daily sea ice concentration data in front of the ice shelf ($24\text{--}34^\circ\text{E}$, $71\text{--}68^\circ\text{S}$) during 2016 are generated based on the satellite passive microwave-derived data sets (Fetterer et al., 2017). Sea ice index data are provided by the National Snow and Ice Data Center.

Seasonal variations in the open ocean coastal hydrography are obtained from climatological data presented by Hattermann (2018), which is based on conductivity-temperature-depth (CTD) profiles from ships and Satellite Relay Data Logger-equipped seals (SRDL-CTD) (Boehme et al., 2009) collected near the continental shelf break in the Kapp Norvegia region $10\text{--}25^\circ\text{E}$, $68\text{--}74^\circ\text{S}$ in the period from 1977 to 2016 (Hattermann,

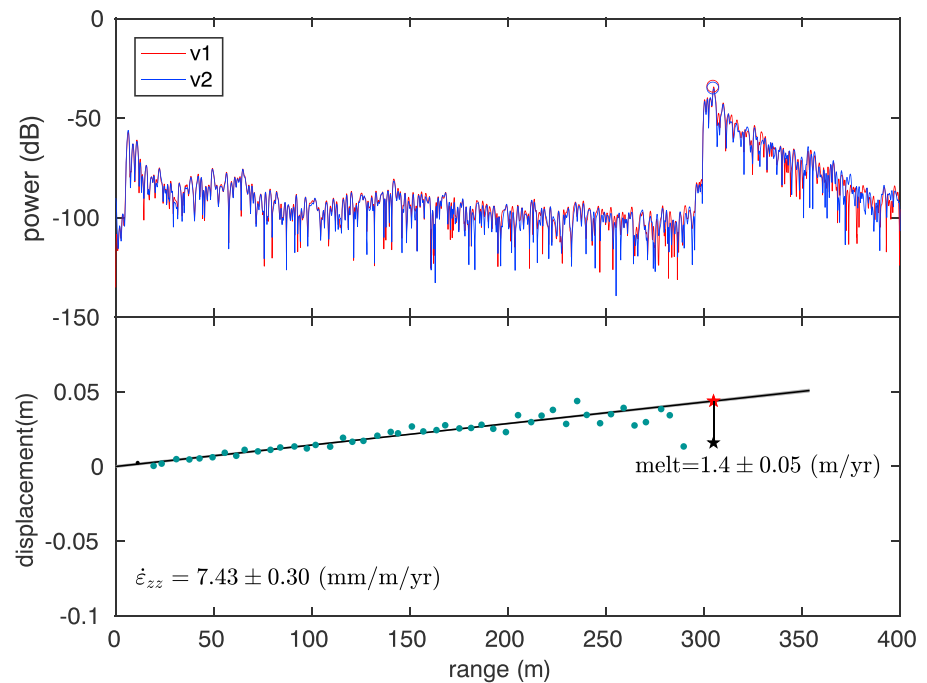


Figure 2. Example of a melt rate calculation for ApRES based on two visits with a 7-day interval. The top panel shows radar records of the initial measurements (blue) and their corresponding remeasurements (red). The circles label the reflection from the ice shelf base. The bottom panel shows the displacements of the reflecting surfaces and the base. We linearly fit (black line) the displacements (green dots) of reflecting surfaces and calculate the vertical strain rate. The black star marks the observed displacement of the shelf base, while the red star marks the displacement due to vertical strain. ApRES = autonomous phase-sensitive radio-echo sounder.

2018). The full climatological data and the underlying raw CTD data are available via the pangaea repository (www.pangaea.de) and references therein (Hattermann & Rohardt, 2018). Previous studies have shown the coevolution of hydrographic properties along the Dronning Maud Land coast (e.g., Nøst et al., 2011), and the few SRDL-CTD profiles that exist north of the RBIS (Figures S2 and S3 in the supporting information) confirm that the Kapp Norvegia climatology is representative for the open ocean seasonality, despite being located further east. As an external forcing, temporal and spatial strength of tides in the study region are obtained using the CATS2008_opt barotropic tide model (Padman et al., 2008).

Temporal variability of ocean properties below the RBIS are unknown. We therefore present contemporaneously collected data from oceanographic moorings beneath the Fimbul ice shelf (M1 and M3; Hattermann et al., 2012), which is located approximately 1,000 km further west along the Dronning Maud Land coast ($\sim 0^\circ\text{E}$) with a similar configuration and similar magnitude of melt rates (Rignot et al., 2013) as the RBIS. The moored instruments are located at about 200-m depth, a few meters beneath the ice base.

3. Temporal Variability in Subshelf Melting and Ocean Properties

Time series of basal melt rates (Figure 3) are obtained for sliding intervals of both 4 hr and 1 day. That is, we compare pairs of observations separated by 4 hr and separated by 1 day, and then move that interval along by 1 hr.

The observational year 2016 can be divided into three periods corresponding to the phases of the melt rates (Figure 3a): (a) From January to mid-May, the ApRES data set indicates higher average melt rates of up to 10 m/a, as well as a higher variability in melt rates. This period coincides with the sea ice-free season (Figure 3b). (b) From May to August, it changes abruptly to a phase of weak melt/refreezing when the sea ice cover increases at the onset of the winter. (c) From September, the magnitude and the variation of melt rates increase gradually. However, both are much lower than period (a), consistent with a significant sea ice cover during that period.

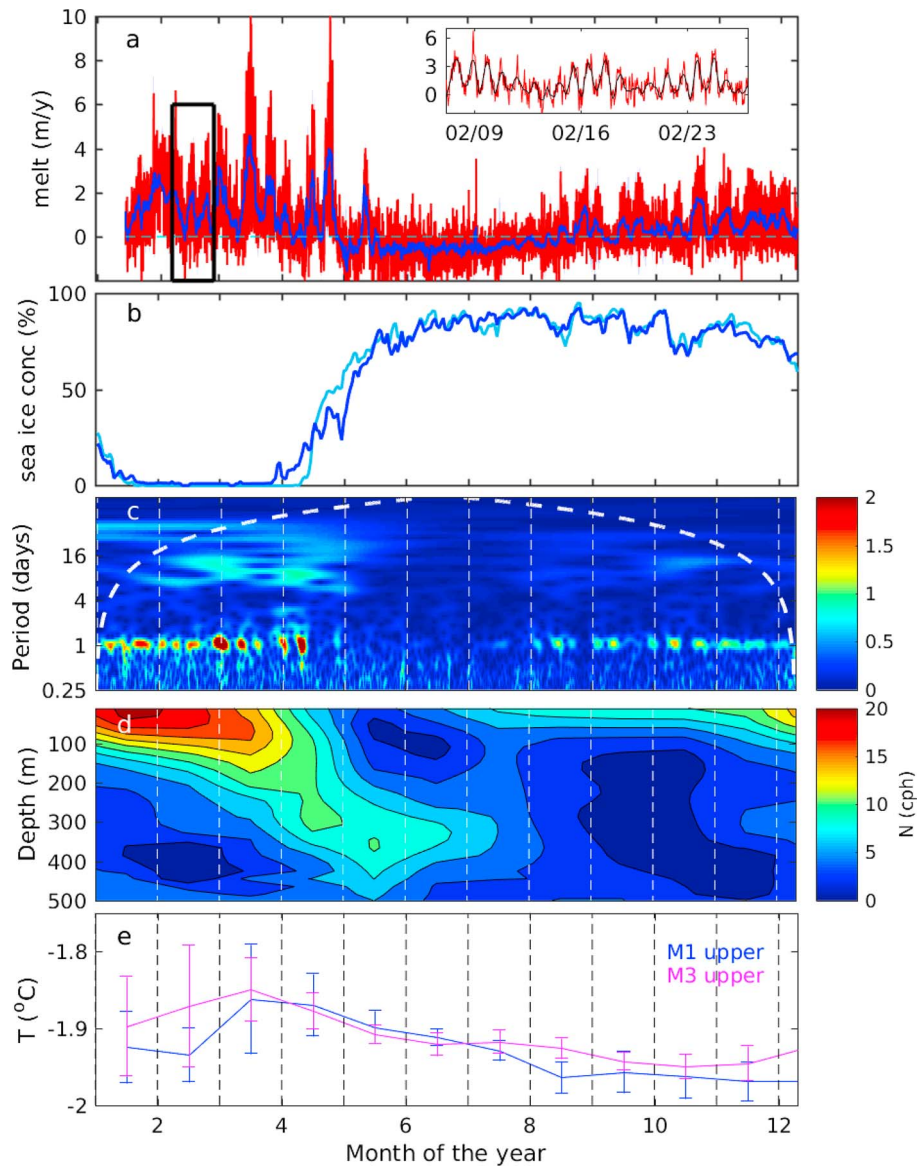


Figure 3. Time series of the observational data sets: (a) Time series of melt rates with 4-hr window (red line), overlaid by time series with 1-day window (blue line). The time series of melt rates with 4-hr window from 7 to 26 February (the black box) is shown in the inset plot (red line), overlaid by the smoothed data (black line) to clearly show the diurnal period; (b) sea ice concentration at the front of the Roi Baudouin Ice Shelf in 2016 between 24° and 34°E in cyan and between 30° and 32°E in blue; (c) periodograms of the melt rates derived using 4-hr moving window. The white dashed line shows the cone of influence; (d) climatological time series of coastal ocean stratification seaward of the ice front at Kapp Norvegia (Hattermann, 2018); (e) time series (monthly mean) of 2016 upper ocean temperatures at two moorings beneath the Fimbul Ice Shelf (near the ice front) at the same location as in Hattermann et al. (2012). The error bars represent the variance within each month of the hourly data (standard deviation).

The evolution of open ocean stratification along the Dronning Maud Land coast is in accord with the three periods above (Figure 3d, see also Figure S2 for time series of temperature and salinity). Strong vertical density gradients in the upper 100–200 m are observed during the sea ice-free period (a) when fresher and solar-heated ASW accumulates along the coast (Zhou et al., 2014). At the onset of the sea ice formation period (b), the stratification abruptly vanishes when brine rejection convectively mixes the water column on the continental shelf. Later during winter (c) when further ice formation is suppressed by a solid ice cover that isolates the ocean from cold atmospheric temperatures, along-shelf advection (Graham et al., 2013) and on-shelf eddy fluxes of MWDW (Nøst et al., 2011) slowly restratify the water column.

The Fimbul Ice Shelf moorings also show a seasonal inflow of solar-heated surface water (Figure 3e), albeit with a different timing because of the delay-associated downwelling of the ASW before it enters the cavity (Zhou et al., 2014). However, the maximum temperatures observed around March and April and the gradual cooling until August/September does not fit well with the abrupt drop in melt rates seen at the ApRES site in mid-April.

To capture signals at higher frequencies (e.g., semidiurnal), we use a sliding, 4-hr interval to obtain the melt rates for the wavelet analysis (Figures 3a and 3c). A generalized Morse wavelet characterized by parameters $\gamma = 3$ and $\beta = 20$ is employed here (Lilly & Olhede, 2009). Melt rate variability at the diurnal periods is dominant and much larger than the semidiurnal periods. However, vertical strain rates express a strong variability at both diurnal and semidiurnal periods (not shown). During summer, there is a secondary maximum in the 8–16 days range in melt rate variability, probably corresponding to the fortnight spring-neap cycle, which can also be seen from the pulsatile signal of the diurnal frequencies. For the whole observed period, the diurnal signal from the ApRES is strong in period (a), vanishes in period (b), and reappears weakly during period (c).

Figure 1 also shows the dominant tidal forcing in the study region. Results from the CATS2008_opt model show a pronounced local amplification of diurnal tides over the Gunnerus Bank, with K1 tidal velocities of over 20 cm/s being an order of magnitude larger than generally found along the shelf break in the area (Figure 1). Moreover, the second major diurnal constituent O1 shows a similar pattern, while amplitudes of the semidiurnal frequencies in contrast are much lower, with current velocities not exceeding a few centimeters per second and no pronounced amplification over the Gunnerus Bank being seen in tidal model (Figure S1). This asymmetry is attributed to the generation of topographically trapped diurnal vorticity waves that have been reported in other regions along the Antarctic continental shelf break (e.g., Middleton et al., 1987; Padman & Kottmeier, 2000; Padman et al., 2003) and also associated with divergent topography as shown by Skarohamar et al. (2015).

4. Discussion

The coincidence of higher melt rates and the absence of sea ice indicates a nearly instantaneous link between the melt rates and the seasonal changes in the oceanic environment seaward of the ice front. Downwelling of solar-heated ASW in the sea ice-free period has been observed to enhance basal melting (Hattermann et al., 2012, 2014), and models suggest that this mechanism is a general feature of the narrow continental shelf configuration with easterly winds (Zhou et al., 2014). However, it is questionable that this process will affect the deeper parts of the cavity to instantaneously increase melt rates near the grounding line. ASW is usually formed in a relatively thin surface layer when sea ice melts. It gradually spreads beneath ice shelf with much of the warming signal being lost on its way into the cavity, as also seen from the rather moderate temperature increase at the Fimbul moorings (Figure 3e). The moorings are both shallower and closer to the open ocean than the ApRES measurements in this study obtained at 300-m depth 90 km away from the ice shelf front.

Instead of relating the melt rates to the lateral advection of warmer water, we suggest that the observed variability is controlled by the seasonal presence of baroclinic waves inside the cavity that modulate the vertical heat flux toward the ice base. In this mechanism, topographically trapped vorticity waves generated by diurnal tides over sloping topography provide energy to excite internal waves that propagate along the slopes of the grounding line toward the ApRES site. The melt rate variability observed beneath RBIS closely follows the upper open ocean stratification and the wavelet analysis indicates that the local circulation is more energetic at diurnal than at semidiurnal frequencies (Figure 3c). Together with the strong diurnal tidal forcing over the Gunnerus Bank (Figure 1), this supports the hypothesis of seasonal resonance of internal waves beneath the ice shelf. In particular, the abrupt termination of the diurnal melt rate signal at the onset of sea ice formation stands out and is hard to explain by other mechanisms than a ceasing of those waves as convection mixes the water column, before a gradual restratification during winter allows baroclinic waves to be generated and transmitted once again.

Unlike freely propagating, semidiurnal modes, the diurnal topographic waves associated with the barotropic tides over the Gunnerus Bank are trapped, that is, they cannot propagate, because they are poleward of the critical latitude, and their conversion into internal waves may be important to facilitate the resonance of these modes inside the ice shelf cavity. Nonlinear and linear examples of propagating baroclinic waves

at above-critical latitudes exist (Hughes & Klymak, 2019; Rippeth et al., 2017) and comparable seasonal resonances of baroclinic waves with diurnal tides have been observed at similar configurations along the Antarctic continental slope (Jensen et al., 2013; Semper & Darelius, 2017). Idealized models that have been used to quantify the internal wave energy rely on constant geometry assumptions, which is challenging for the complex and partially unknown bathymetry around the Riiser-Larsen Peninsula and beneath the RBIS. However, Falahat and Nycander (2015) find that Gunnerus Bank experiences some of the highest energy densities of bottom-trapped internal tides around the Antarctic continent. Furthermore, the 100- to 200-m step change in water column thickness at the ice shelf's calving front imposes a strong potential vorticity barrier that would hamper cross-ice front transport in a vertically well-mixed ocean (Nicholls et al., 2009). The conversion to internal waves may be important in overcoming that barrier. Vertical density gradients at the depth of the ice shelf base may decouple the lower part of the water column, effectively weakening the potential vorticity barrier and allowing baroclinic signals to propagate from the open ocean into the cavity. Such decoupling by summer time stratification has been evoked to explain the exchange across ice fronts at other ice shelves (Darelius & Sallée, 2018; Malyarenko et al., 2019; Nicholls et al., 2009). With wavelengths usually in the order of a few hundred kilometers for the first modes, the resulting internal waves may well resonate with the size of the ice shelf cavity, causing a nearly instantaneous response to open ocean signals along the grounding line from the outcrop to the open ocean at the Riiser-Larsen Peninsula toward the ApRES.

The observed basal melt rates are essentially controlled by the local thermal driving and the friction velocity (Holland & Jenkins, 1999). The presence of energetic waves would increase both of these two factors by enhancing the upward mixing of heat in the ambient ocean and by increasing turbulence at the ice-ocean interface. Herein, the observed magnitude of the summer peak melt rates suggests that a significant amount of water somewhat warmer than the surface freezing point is available in the cavity to be raised by tidal activity. While the bathymetry beneath RBIS is largely unknown, warmer inflows at depth may also affect the melt rate variability. Hattermann (2018) suggested that the presence of ASW along the coast of Dronning Maud Land causes a shoaling of the thermocline along the shelf break that may cause seasonal access of warmer water over sills and troughs into the ice shelf cavity. Although such intermittent inflows probably play a role in providing ocean heat for melting inside the cavity, large variations in this process would likely leave more gradual and somewhat delayed signature in the melt rate signal at the grounding line than the observed variability that appears to be phase locked with the sea ice-free period as is consistent with the topographic wave argument.

Finally, if tides and topographic waves beneath RBIS would have the same characteristics all year round, the wavelet analysis in Figure 3c would show an enhancement of the diurnal frequency interval also during the sea ice formation period, as melt rate variability in Figure 3a is not zero at that time. Instead, most of the variability seems to occur at higher frequencies, suggesting the absence of a pronounced diurnal signal in the exchange velocities at the ice-ocean boundary.

5. Conclusions

Based on continuous ApRES measurements, we provide a yearlong, hourly time series of directly measured subshelf melt rates that enable us to investigate temporal variability of subshelf melt rates at a broad range of time scales.

The magnitude of subshelf melt rates varies from close to 0 in winter to 10 m/a in summer, with variations over a broad range of time scales, from tidal to seasonal. We propose that the subshelf melt rate of the RBIS near its grounding line is controlled by topographic waves triggered over the Gunnerus Bank. By controlling the turbulent mixing of heat and salt toward the ice shelf base, topographic waves directly affect the local melt rates and act as a conduit for propagating open ocean changes to the grounding line far inside the ice shelf cavity, even without advecting different water masses beneath the ice shelf. Such topographic waves are observed to resonate with the diurnal tides at the Antarctic continental slope (Semper & Darelius, 2017), but their resonance depends on the stratification in the upper water column, leading to a seasonal variation in the strength of waves, which, in turn, leads to the seasonally varying strength of the diurnal signal in the melt rate time series. The formation and decline of sea ice therefore impacts the melt rates indirectly by modulating the stratification of the ocean.

Although the detailed dynamics of the internal waves inside the RBIS cavity will need to be explored in future studies, our observations suggest a mechanism for regulating ice shelf basal melting that has not previously been considered. It seems to dominate the melt variability along parts of the grounding line at the RBIS and will likely be present beneath other ice shelves along the Dronning Maud Land coast. In this process, open ocean bathymetry and far-field tidal and surface forcing plays a key role in controlling melt variability deep inside the cavity. It may also be important for modulating the melt rate response to future climate change, as observations and models suggest an ongoing freshening of ASW (de Lavergne et al., 2014). Recent studies based on fully coupled ice-ocean-atmospheric modeling show that the melt water flux from Antarctica will trap warm water below the sea surface, in turn increase the melting near the grounding line and create a positive feedback (Bronse laer et al., 2018; Golledge et al., 2019; Menviel et al., 2010). Increasing melt water fluxes will further increase the (winter time) stratification of continental shelf waters, and in case of the RBIS, this will likely enhance the presence of topographic waves and permanently increase the heat flux and melt rates near the grounding line of the ice shelf.

Acknowledgments

We thank X. Asay-Davis and the anonymous reviewer for their constructive comments. This paper forms a contribution to the Belgian Research Programme on the Antarctic (Belgian Federal Science Policy Office), project SD/CA/06A (Constraining Ice Mass Change in Antarctica, IceCon) and the FNRS-PDR (Fonds de la Recherche Scientifique) project MEDRISM and the BELSPO MIMO project (Stereo III). We received excellent logistic support by the Belgian Military, AntarctiQ and the International Polar Foundation during the field campaigns. R. Drews was partially supported by the DFG Emmy Noether Grant DR 822/3-1. The time series of melt rates are available via pangaea repository (<https://doi.pangaea.de/10.1594/PANGAEA.903182>). We would like to thank Laura de Steur (Norwegian Polar Institute) for providing the mean seasonal cycle from the Fimbul Ice Shelf mooring data, which are available via (<https://data.npolar.no>) upon request.

References

- Bindschadler, R., Choi, H., Wichlacz, A., Bingham, R., Bohlander, J., Brunt, K., et al. (2011). Getting around Antarctica: New high-resolution mappings of the grounded and freely-floating boundaries of the Antarctic ice sheet created for the International Polar Year. *Cryosphere*, 5(3), 569–588. <https://doi.org/10.5194/tc-5-569-2011>
- Boehme, L., Lovell, P., Biuw, M., Roquet, F., Nicholson, J., Thorpe, S. E., et al. (2009). Technical Note: Animal-borne CTD-Satellite Relay Data Loggers for real-time oceanographic data collection. *Ocean Science*, 5, 685–695. <https://doi.org/10.5194/os-5-685-2009>
- Brennan, P. V., Nicholls, K., Lok, L. B., & Corr, H. (2014). Phase-sensitive FMCW radar system for high-precision Antarctic ice shelf profile monitoring. *IET Radar, Sonar & Navigation*, 8(7), 776–786. <https://doi.org/10.1049/iet-rsn.2013.0053>
- Bronse laer, B., Winton, M., Griffies, S. M., Hurlin, W. J., Rodgers, K. B., Sergienko, O. V., et al. (2018). Change in future climate due to Antarctic meltwater. *Nature*, 564, 53–58. <https://doi.org/10.1038/s41586-018-0712-z>
- Callens, D. (2014). Impact of improved basal and surface boundary conditions on the mass balance of the Sør Rondane Mountains glacial system, Dronning Maud Land, Antarctica (PhD Thesis), ULB. 75pp.
- Callens, D., Matsuoka, K., Steinhage, D., Smith, B., Witrant, E., & Pattyn, F. (2014). Transition of flow regime along a marine-terminating outlet glacier in East Antarctica. *The Cryosphere*, 8, 867–875. <https://doi.org/10.5194/tc-8-867-2014>
- Corr, H. F. J., Jenkins, A., Nicholls, K. W., & Doake, C. S. M. (2002). Precise measurement of changes in ice-shelf thickness by phase-sensitive radar to determine basal melt rates. *Geophysical Research Letters*, 29(8), 1232. <https://doi.org/10.1029/2001GL014618>
- Darelius, E., & Sallée, J. B. (2018). Seasonal outflow of ice shelf water across the front of the Filchner ice shelf, Weddell Sea, Antarctica. *Geophysical Research Letters*, 45, 3577–3585. <https://doi.org/10.1002/2017GL076320>
- Davis, P. E. D., Jenkins, A., Nicholls, K. W., Brennan, P. V., Povl Abrahamsen, E., & Heywood, K. J. (2018). Variability in basal melting beneath Pine Island Ice Shelf on weekly to monthly timescales. *Journal of Geophysical Research: Oceans*, 123, 8655–8669. <https://doi.org/10.1029/2018JC014464>
- de Lavergne, C., Palter, J. B., Galbraith, E. D., Bernardello, R., & Marinov, I. (2014). Cessation of deep convection in the open southern ocean under anthropogenic climate change. *Nature Communications*, 4, 278–282. <https://doi.org/10.1038/nclimate2132>
- Depoorter, M. A., Bamber, J. L., Griggs, J. A., Lenaerts, J. T. M., Ligtenberg, S. R. M., van den Broeke, M. R., & Moholdt, G. (2013). Calving fluxes and basal melt rates of Antarctic ice shelves. *Nature*, 502(7469), 89–92. <https://doi.org/10.1038/nature12567>
- Dinniman, M. S., Asay-Davis, X. S., Galton-Fenzi, B. K., Holland, P. R., Jenkins, A., & Timmermann, R. (2016). Modeling ice shelf/ocean interaction in Antarctica: A review. *Oceanography*, 29(4), 144–153. <https://doi.org/10.5670/oceanog.2016.106>
- Dong, J., Speer, K., & Jullion, L. (2016). The antarctic slope current near 30 E. *Journal of Geophysical Research: Oceans*, 121, 1051–1062. <https://doi.org/10.1002/2015JC011099>
- Drews, R. (2015). Evolution of ice-shelf channels in Antarctic ice shelves. *The Cryosphere*, 9, 1169–1181. <https://doi.org/10.5194/tc-9-1169-2015>
- Dupont, T. K., & Alley, R. B. (2005). Assessment of the importance of ice-shelf buttressing to ice-sheet flow. *Geophysical Research Letters*, 32, L04503. <https://doi.org/10.1029/2004GL022024>
- Falahat, S., & Nycander, J. (2015). On the Generation of Bottom-Trapped Internal Tides. *Journal of Physical Oceanography*, 45, 526–545. <https://doi.org/10.1175/JPO-D-14-0081.1>
- Favier, L., Durand, G., Cornford, S. L., Gudmundsson, G. H., Gagliardini, O., Gillet-Chaulet, F., et al. (2014). Retreat of Pine Island Glacier controlled by marine ice-sheet instability. *Nature Climate Change*, 5(2), 117–121. <https://doi.org/10.1038/nclimate2094>
- Favier, L., Pattyn, F., Berger, S., & Drews, R. (2016). Dynamic influence of pinning points on marine ice-sheet stability: A numerical study in Dronning Maud Land, East Antarctica. *The Cryosphere*, 10, 2623–2635. <https://doi.org/10.5194/tc-10-2623-2016>
- Fetterer, F., Knowles, K., Meier, W., Savoie, M., & Windnagel, A. K. (2017). Updated daily. Sea Ice Index, Version 3. NSIDC: National Snow and Ice Data Center. <https://doi.org/10.7265/N5K072F8>
- Fretwell, P., Pritchard, H. D., Vaughan, D. G., Bamber, J. L., Barrand, N. E., Bell, R., et al. (2013). Bedmap2: Improved ice bed, surface and thickness datasets for Antarctica. *The Cryosphere*, 7, 375–393. <https://doi.org/10.5194/tc-7-375-2013>
- Golledge, N. R., Keller, E. D., Gomez, N., Naughten, K. A., Bernales, J., Trusel, L. D., & Edwards, T. L. (2019). Global environmental consequences of twenty-first-century ice-sheet melt. *Nature*, 566(7742), 65–72. <https://doi.org/10.1038/s41586-019-0889-9>
- Graham, A. G. C., Dutrieux, P., Vaughan, D. G., Nitsche, F. O., Gyllencreutz, R., Greenwood, S. L., et al. (2013). Seabed corrugations beneath an Antarctic ice shelf revealed by autonomous underwater vehicle survey: Origin and implications for the history of Pine Island Glacier. *Journal of Geophysical Research: Earth Surface*, 118, 1356–1366.
- Hattermann, T. (2018). Antarctic Thermocline Dynamics along a Narrow Shelf with Easterly Winds. *Journal of Physical Oceanography*, 48, 2419–2443. <https://doi.org/10.1175/JPO-D-18-0064.1>
- Hattermann, T., Nøst, O. A., Lilly, J. M., & Smedsrud, L. H. (2012). Two years of oceanic observations below the Fimbul ice shelf, Antarctica. *Geophysical Research Letters*, 39, L12605. <https://doi.org/10.1029/2012GL051012>

- Hattermann, T., Smedsrud, L. H., Nøst, O. A., Lilly, J. M., & Galton-Fenzi, B. K. (2014). Eddy-resolving simulations of the Fimbul Ice Shelf cavity circulation: Basal melting and exchange with open ocean. *Ocean Modelling*, *82*, 28–44.
- Hattermann, T., & Rohardt, G. (2018). Kapp Norvegia Antarctic Slope Front climatology. <https://doi.org/10.1594/PANGAEA.893199>
- Heywood, K. J., Locarnini, R. A., Frew, R. D., Dennis, P. F., & King, B. A. (1998). Transport and water masses of the antarctic slope front system in the eastern weddell sea. In S. S. Jacobs, & R. F. Weiss (Eds.), *Ocean, ice and atmosphere: Interactions at the antarctic continental margin* pp. 203–214. Washington, DC: American Geophysical Union.
- Holland, P. R., & Jenkins, A. (1999). Modelling thermodynamic ice-ocean interactions at the base of an ice shelf. *Journal of Physical Oceanography*, *29*, 1787–1800.
- Howat, I. M., Porter, C., Smith, B. E., Noh, M.-J., & Morin, P. (2019). The reference elevation model of antarctica. *The Cryosphere*, *13*, 665–674. <https://doi.org/10.5194/tc-13-665-2019>
- Hughes, K. G., & Klymak, J. M. (2019). Tidal conversion and dissipation at steep topography in a channel poleward of the critical latitude. *Journal of Physical Oceanography*, *49*, 1269–1291. <https://doi.org/10.1175/JPO-D-18-0132.1>
- Jacobs, S., Helmer, H., Doake, C., Jenkins, A., & Frolich, R. (1992). Melting of ice shelves and the mass balance of Antarctica. *Journal of Glaciology*, *38*(130), 375–387. <https://doi.org/10.1017/S002214300002252>
- Jenkins, A., Corr, H. F. J., Nicholls, K. W., Stewart, C. L., & Doake, C. S. M. (2006). Interactions between ice and ocean observed with phase-sensitive radar near an Antarctic ice-shelf grounding line. *Journal of Glaciology*, *52*(178), 325–346. <https://doi.org/10.3189/172756506781828502>
- Jenkins, A., & Doake, C. S. M. (1991). Ice-ocean interaction on ronne ice shelf, antarctica. *Journal of Geophysical Research*, *96*(C1), 791–813.
- Jensen, M. F., Fer, I., & Darelus, E. (2013). Low frequency variability on the continental slope of the southern weddell sea. *Journal of Geophysical Research: Oceans*, *118*, 4256–4272. <https://doi.org/10.1002/jgrc.20309>
- Jezeq, K., & RAMP-Product-Team (2002). RAMP AMM-1 SAR Image Mosaic of Antarctica. Fairbanks, AK: Alaska Satellite Facility, in association with the National Snow and Ice Data Center, Boulder, CO. Digital media.
- Jourdain, N. C., Molines, J., Le Sommer, J., Mathiot, P., Chanut, J., de Lavergne, C., & Madec, G. (2019). Simulating or prescribing the influence of tides on the Amundsen Sea ice shelves. *Ocean Modelling*, *133*, 44–55. <https://doi.org/10.1016/j.ocemod.2018.11.001>
- Lenaerts, J. T. M., Lhermitte, S., Drews, R., Ligtenberg, S. R. M., Berger, S., Helm, V., et al. (2016). Meltwater produced by wind–albedo interaction stored in an east antarctic ice shelf. *Nature Climate Change*, *7*(1), 58–62. <https://doi.org/10.1038/nclimate3180>
- Lewis, E. L., & Perkin, R. G. (1986). Ice pumps and their rates. *Journal of Geophysical Research*, *91*(C10), 11,756–11,762. <https://doi.org/10.1029/JC091iC10p11756>
- Lilly, J. M., & Olhede, S. C. (2009). Higher-order properties of analytic wavelets. *IEEE Transactions on Signal Processing*, *57*(1), 146–160.
- Makinson, K., Holland, P. R., Jenkins, A., Nicholls, K. W., & Holland, D. M. (2011). Influence of tides on melting and freezing beneath filchner-ronne ice shelf, antarctica. *Geophysical Research Letters*, *38*, L06601. <https://doi.org/10.1029/2010GL046462>
- Malyarenko, A., Robinson, N. J., Williams, M. J. M., & Langhorne, P. J. (2019). A wedge mechanism for summer surface water inflow into the ross ice shelf cavity. *Journal of Geophysical Research: Oceans*, *124*, 1196–1214. <https://doi.org/10.1029/2018JC014594>
- Menviel, L., Timmermann, A., Timm, O. E., & Mouchet, A. (2010). Climate and biogeochemical response to a rapid melting of the West Antarctic Ice Sheet during interglacials and implications for future climate. *Paleoceanography*, *25*, PA4231. <https://doi.org/10.1029/2009PA001892>
- Middleton, J. H., Foster, T. D., & Foldvik, A. (1987). Diurnal Shelf Waves in the Southern Weddell Sea. *Journal of Physical Oceanography*, *17*, 784–791.
- Nicholls, K. W., Corr, H. F. J., Stewart, C. L., Lok, L. B., Brennan, P. V., & Vaughan, D. G. (2015). Instruments and methods: A ground-based radar for measuring vertical strain rates and time-varying basal melt rates in ice sheets and shelves. *Journal of Glaciology*, *61*(230), 1079–1087. <https://doi.org/10.3189/2015JoG15J073>
- Nicholls, K. W., Østerhus, S., Makinson, K., Gammelsrød, T., & Fahrbach, E. (2009). Ice-ocean processes over the continental shelf of the southern Weddell Sea, Antarctica: A review. *Review of Geophysics*, *47*, RG3003. <https://doi.org/10.1029/2007RG000250>
- Nøst, O. A., Biuw, M., Tverberg, V., Lydersen, C., Hattermann, T., Zhou, Q., et al. (2011). Eddy overturning of the antarctic slope front controls glacial melting in the eastern weddell sea. *Journal of Geophysical Research*, *116*, C11014. <https://doi.org/10.1029/2011JC006965>
- Padman, L., Erofeeva, S. Y., & Fricker, H. A. (2008). Improving Antarctic tide models by assimilation of ICESat laser altimetry over ice shelves. *Geophysical Research Letters*, *35*, L22504. <https://doi.org/10.1029/2008GL035592>
- Padman, L., Erofeeva, S., & Joughin, I. (2003). Tides of the Ross Sea and Ross Ice Shelf cavity. *Antarctic Science*, *15*(01), 31–40.
- Padman, L., & Kottmeier, C. (2000). High-frequency ice motion and divergence in the Weddell Sea. *Journal of Geophysical Research*, *105*(C2), 3379–3400. <https://doi.org/10.1029/1999JC900267>
- Padman, L., Siegfried, M. R., & Fricker, H. A. (2018). Ocean tide influences on the Antarctic and Greenland ice sheets. *Reviews of Geophysics*, *56*, 142–184. <https://doi.org/10.1002/2016RG000546>
- Rack, W., & Rott, H. (2004). Pattern of retreat and disintegration of the larsen b ice shelf, antarctic peninsula. *Annals of Glaciology*, *39*, 505–510. <https://doi.org/10.3189/172756404781814005>
- Reese, R., Gudmundsson, G. H., Levermann, A., & Winkelmann, R. (2018). The far reach of ice-shelf thinning in Antarctica. *Nature Climate Change*, *8*, 53–57. <https://doi.org/10.1038/s41558-017-0020-x>
- Rignot, E., Jacobs, S., Mougnot, J., & Scheuchl, B. (2013). Ice-Shelf Melting Around Antarctica. *Science*, *1455*(1988), 2008–2011. <https://doi.org/10.1126/science.1235798>
- Rippeth, T. P., Vlasenko, V., Stashchuk, N., Scannell, B. D., Green, J. A. M., Lincoln, B. J., & Bacon, S. (2017). Tidal conversion and mixing poleward of the critical latitude (an Arctic case study). *Geophysical Research Letters*, *44*, 12,349–12,357. <https://doi.org/10.1002/2017GL075310>
- Schannwell, C., Cornford, S., Pollard, D., & Berrand, N. E. (2018). Dynamic response of antarctic peninsula ice sheet to potential collapse of larsen c and george vi ice shelves. *The Cryosphere*, *12*(7), 2307–2326. <https://doi.org/10.5194/tc-12-2307-2018>
- Semper, S., & Darelus, E. (2017). Seasonal resonance of diurnal coastal trapped waves in the southern weddell sea, antarctica. *Ocean Science*, *13*, 77–93. <https://doi.org/10.5194/os-13-77-2017>
- Skarohamar, J., Skagseth, Ø., & Albretsen, J. (2015). Diurnal tides on the barents sea continental slope. *Deep-Sea Research*, *97*, 40–51. <https://doi.org/10.1016/j.dsr.2014.11.008>
- Stewart, A. L., Klocker, A., & Menemenlis, D. (2018). Circum-Antarctic shoreward heat transport derived from an eddy- and tide-resolving simulation. *Geophysical Research Letters*, *45*, 834–845. <https://doi.org/10.1002/2017GL075677>
- Weatherall, P., Marks, K. M., Jakobsson, M., Schmitt, T., Tani, S., Arndt, J. E., et al. (2015). A new digital bathymetric model of the world's oceans. *Earth and Space Science*, *2*, 331–345. <https://doi.org/10.1002/2015EA000107>
- Zhou, Q., Hattermann, T., Nø, O. A., Biuw, M., Kovacs, K. M., & Lydersen, C. (2014). Wind-driven spreading of fresh surface water beneath ice shelves in the eastern weddell sea. *Journal of Geophysical Research: Oceans*, *119*, 3818–3833. <https://doi.org/10.1002/2013JC009556>